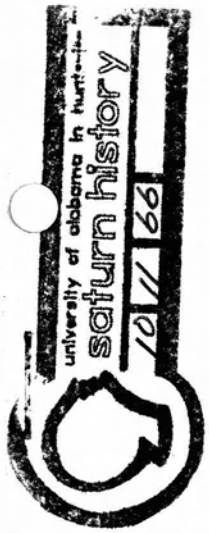

THE USE OF WIND SHEARS IN THE DESIGN OF AEROSPACE VEHICLES

By

Robert S. Ryan and James R. Scoggins

Aero-Astrodynamics Laboratory

George C. Marshall Space Flight Center

National Aeronautics and Space Administration

Huntsville, Alabama

X 1.2

Prepared for Presentation at the
23rd Meeting of the Structures and Materials Panel, AGARD,
October 4 - 11, 1966
ONERA, Paris, France

THE USE OF WIND SHEARS IN THE DESIGN OF AEROSPACE VEHICLES

By

Robert S. Ryan and James R. Scoggins

ABSTRACT

The relative influence of various wind profile properties and disturbances on launch vehicle flight dynamic response is studied. Particular emphasis is placed on the influence of wind shears and turbulence on dynamic response during the boost phase of the flight. Four hundred and seven individual detailed (Jimsphere) wind profiles are the primary wind inputs for this analysis. Time response of the vehicle to each profile is computed and a statistical evaluation of the results made. Results are obtained for the Saturn V space vehicle and conclusions drawn as to the relative influence of wind shears and turbulence vs the degree of refinement of the dynamic model of the space vehicle.

INTRODUCTION

Wind disturbances are one of the major influences on space vehicle design and operations. As these disturbances interact with the vehicle and its control system, various problems arise. Of paramount concern are the resulting unit compression or tension loads which influence the design of the vehicle structure. Another problem is optimization of the vehicle control system. Proper design of the control system produces lower structural loads allowing more payload in orbit and fewer operational restrictions. These restrictions normally arise as wind speed limitations for launching the vehicle.

Assessment of the structural design and control system optimization requires an adequate representation of the wind field, vehicle dynamics, and control system. Accurate methods of analysis, adequate wind inputs, and representative vehicle response parameters for evaluation are of equal importance. This paper satisfies the vehicle representation by using a detailed mathematical model of the total vehicle dynamics. To satisfy the wind field requirements, the low frequency content of the wind (magnitude) has been separated from the high frequency (turbulence). Thus, three profiles are obtained, the unfiltered, filtered, and turbulence, for use in studying vehicle responses.

Solutions of the vehicle responses were obtained using three procedures: numerical integration of the equations of motion, analog computer solution, and for the turbulence portion, generalized harmonic

analysis. Either the bending moment or unit compressive load or both are chosen as the parameter to evaluate the response.

The analysis shows that the inclusion of short duration wind disturbances is significant in both structural design and control system optimization.

Special appreciation is expressed to Mr. Helmut J. Horn for his inspiration and technical leadership, to Mrs. Alberta King for analysis and assistance in documenting information, and to Messrs. Floyd Grissett and Wade Perry for preparation of the illustrations. All of these people are members of the Aero-Astrodynamics Laboratory.

SECTION I. WIND INPUTS FOR SPACE VEHICLE DESIGN

Engineering and statistical representation of the wind field is a major problem facing space vehicle design engineers. This representation greatly influences the vehicle design, requiring close working agreement between meteorologists and vehicle dynamics specialists. This paper is concerned with the isolation of the small duration wind shears from the long duration wind build-up and mean wind speed so that the various influences of wind shears on vehicle response can be studied in detail.

A. Wind Velocity Profile Measurements

1. Rawinsonde (GMD)

The largest single source of wind data available is the rawinsonde (GMD) individual wind profiles. These data have been collected from many locations throughout the world and cover several years of

measurements. (Within the limitations inherent in the measurements, it is the best statistical sample available today.) As a result of the smoothing inherent in this method, small duration wind details are missing (Ref. 1). Wind magnitude as a function of altitude is obtained by averaging over approximately 600 meters in altitude. Approximate RMS errors in wind speed based on standard data reduction procedures vary between approximately 2 and 15 meters per second, depending upon wind conditions and tracking geometry. RMS errors in wind direction are estimated to vary between approximately 5 and 20 degrees. These data serve as a good basis upon which to interpret smaller samples and in constructing synthetic wind profiles.

2. FPS-16 Radar/Jimsphere

The FPS-16 Radar/Jimsphere approach to obtaining wind data provides considerably more accurate wind velocity profile data than does the rawinsonde. The measurements are averaged over 25 to 50 meters in the vertical with an RMS error in wind speed of approximately 0.5 meters per second and 1 degree in wind direction (Refs. 2 & 3). Thus, these wind profile data contain information on small-scale motions as well as gross motions such as provided by the rawinsonde. Almost two years of profile data measured twice daily are available from the Kennedy Space Center, Florida. Additional data are also available from the Pacific Missile Range, California and the White Sands Missile Range, New Mexico.

The Wind Shear Working Group of the Structures and Materials Panel considered the problem of documentation of detailed wind velocity profile measurements and concluded that it would be desirable to

present them in graphical and tabular forms, and store the data on a master magnetic tape for easy access. These goals are being met for the data measured in the United States (Ref. 4). Both the tabular forms and tapes were used in the analysis for this report.

B. Short Duration Gusts Associated with Wind Velocity Profiles

Meaningful interpretation of the vehicle reaction to the short duration wind gusts can be made only if an adequate definition and isolation of the disturbing function can be made.

Definition

An adequate definition has not yet been developed. The definition of gusts depends upon the characteristics of the vehicle system considered, such as mass and its distribution, aerodynamics, control system characteristics, etc. Thus, what might be considered as a good definition of gusts or turbulence for a particular vehicle might not be a good definition for a different vehicle. The definition of gusts determines the statistical distribution of the turbulence field and influences the interpretation of results obtained.

An attempt has been made to define gusts (turbulence) in a meaningful way by separating a detailed wind velocity profile into three profiles on the basis of frequency content. The basic profile represents the total wind field, the filtered profile represents the quasi-steady-state wind speeds, and the difference between these two represents gusts or turbulence. Determination of the wind content to be filtered out of the total wind profile is made by giving consideration to relationships between the rawinsonde and FPS-16 radar/Jimsphere profiles plus frequency

response characteristics of the vehicle to be used (in this case the Saturn V). The statistical properties of the gust profile, such as normality and stationarity, were also considered. A filter function is defined so the resulting filtered profile approximates the rawinsonde measured profile. The filter function used in this study is shown in Figure 1 as a function of gust wave length (Ref. 5).

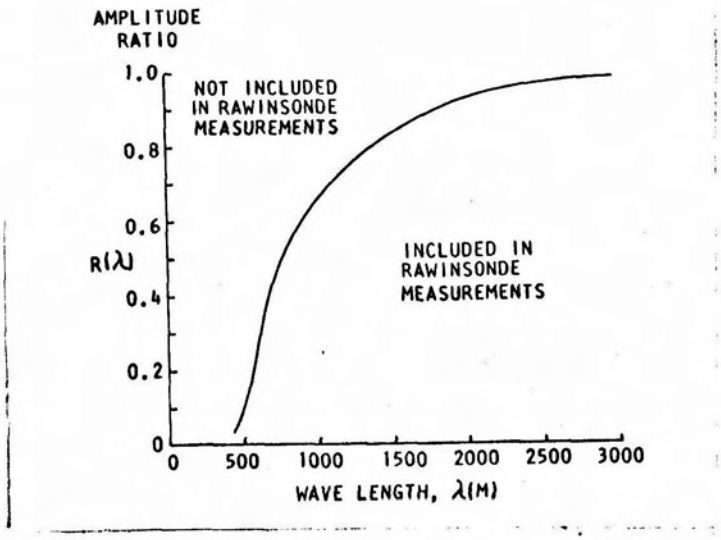

Figure 1. Approximate Response Function for Rawinsonde (GMD-1B) System Based on Standard Rawinsonde Reduction Technique

The separated gust or turbulent profile contains frequencies that cover the whole frequency spectrum of the elastic vehicle.

The statistical distribution of the gusts is approximately Gaussian, enhancing interpretation of the vehicle responses, and also providing a basis for assessing the influence of gusts on the vehicle which are not measured by the rawinsonde method.

This study uses a sample of 407 detailed wind velocity profiles measured by the FPS-16 radar/Jimsphere system; synthetic wind profiles are also used to some extent. The Jimsphere profiles are separated into gusts (turbulence ensemble), quasi-steady-state (filtered ensemble), and total wind profiles (unfiltered ensemble), using the filter function shown above. A typical set of these profiles for one wind measurement is presented in Figures 2 and 3. The time scale is shifted one second between the filtered and unfiltered profiles to prevent overlap in plotting of the profiles.

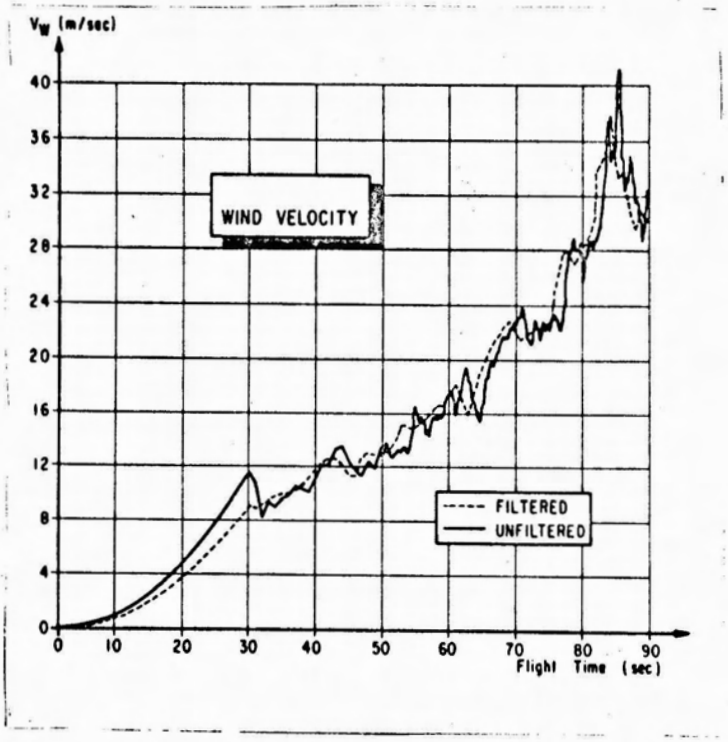

Figure 2. Unfiltered and Filtered Wind Profiles

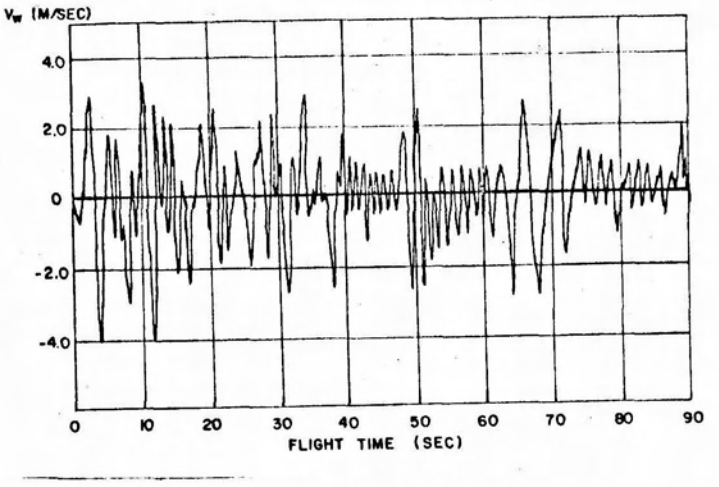

Figure 3. Turbulence Wind Profile

C. Spectra of Short Duration Gusts (Turbulence)

As defined above, the gust profiles represent the motions included in the FPS-16 radar/Jimsphere measurements which are not included in the standard rawinsonde measurements. Therefore, spectra of the motions should be added to the quasi-steady-state wind speed profiles to obtain a representation of the detailed wind profile. The average spectrum of the small-scale motions associated with scalar (without regard to direction) wind profiles is presented in Figure 4 (Ref. 6).

This spectrum was computed from the 407 detailed wind profile measurements by computing the spectrum associated with each profile, then determining the average spectral density as a function of frequency. The spectrum has been transformed from wave numbers to frequency in vehicle flight time near the maximum dynamic pressure region. The spectrum associated with each profile was computed over the entire altitude range of the data, usually between approximately 2 and 16 km. This spectrum is used as input in computing space vehicle responses.

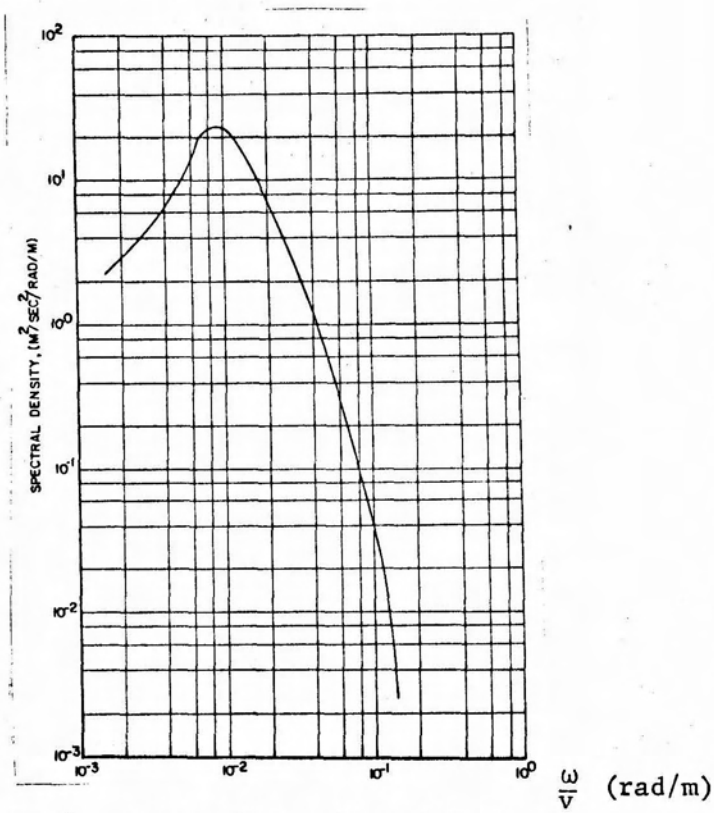

Figure 4. Spectral Density of Turbulence

D. Synthetic Wind Profiles

A synthetic wind profile is an attempt to substitute one representative wind profile for a multitude of measured or statistically defined wind profiles to insure an adequate vehicle design based on the established design philosophy (Ref. 6). Synthetic wind profiles for space vehicle design are usually based on quasi-steady-state wind speeds, wind shears, and gusts, which are combined to represent physically reasonable conditions to insure a high probability of success when the vehicle is launched.

Synthetic wind profiles are constructed by defining the quasi-steady-state wind profile envelope that is not exceeded more than, for instance, 5 percent of the time during some reference period, then defining a wind buildup rate whose envelope is not exceeded more than, say, 1 percent of the time during the reference period, and combining these two in a suitable fashion. Gusts are then superimposed on top of the steady-state wind speed envelope. An idealized quasi-steady-state wind speed envelope representing the 95 percent probability of occurrence using a monthly reference period is shown in Figure 5.

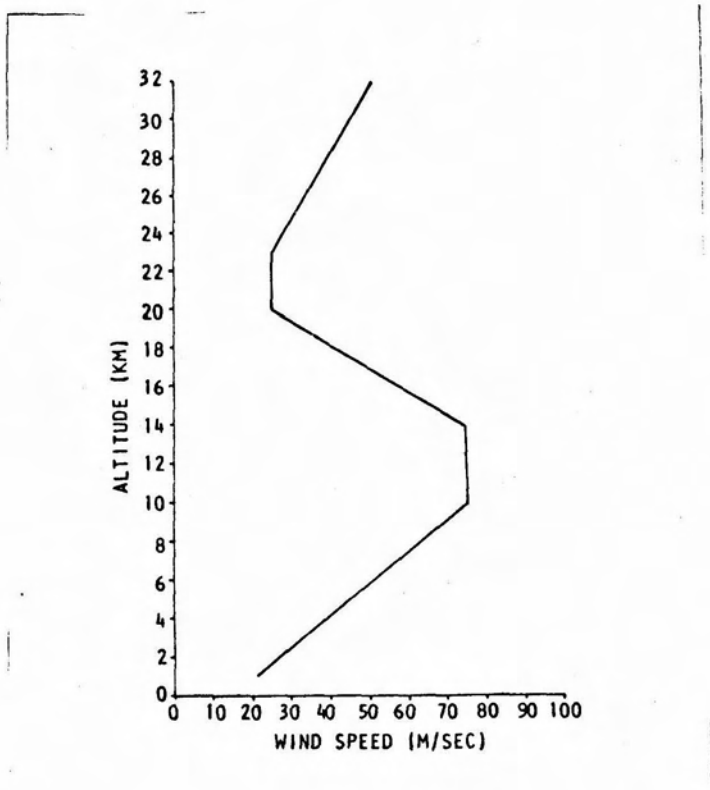

Figure 5. Ninety-Five Percentile Scalar Wind Speed Profile Envelope for Eastern Test Range

This profile was established from several years of rawinsonde data measured at the Eastern Test Range, Florida. Envelopes of the 99 percent probability of occurrence wind speed change for various wind speeds are shown in Figure 6. These wind speed change envelopes were established by computing the wind speed change that occurs below a

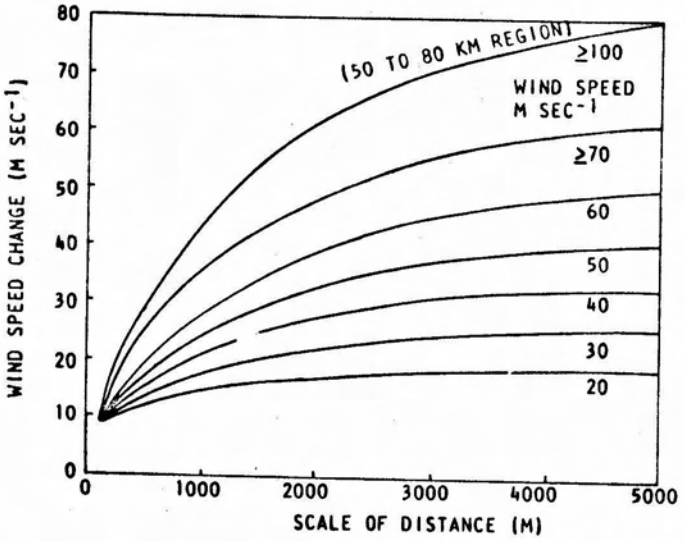

Figure 6. Envelopes of 99 Percentile Wind Speed Change (m sec^{-1}) for Various Scales-of-Distance Corresponding to Wind Speeds at Top of Shear Interval

given (reference) altitude when the quasi-steady-state wind speed at the reference altitude is in one of the ranges shown in the figure, then drawing an envelope of these wind speed change values. This envelope is not intended to imply perfect correlation between the shears over the various altitude intervals.

The quasi-steady-state inflight wind speed envelope presented in Figure 5 does not contain gusts (high frequency content) of the wind profile. The quasi-steady-state wind profile measurements have been defined as those obtained by the rawinsonde system. Therefore, a gust must be superimposed on the quasi-steady-state wind profile to account for the small-scale motions eliminated by the rawinsonde system. The gust which is used for this purpose is shown in Figure 7.

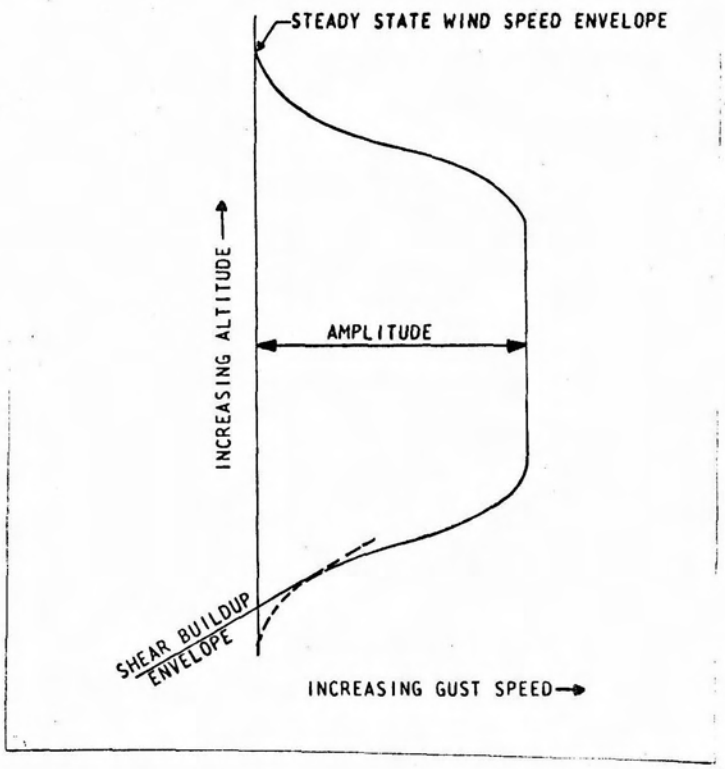

Figure 7. Gust and Its Relationship to the Steady-State Wind Speed and Wind Shear Buildup Envelopes

An example of the construction of synthetic wind profiles without the gust superimposed is shown in Figure 8 (Ref. 6).

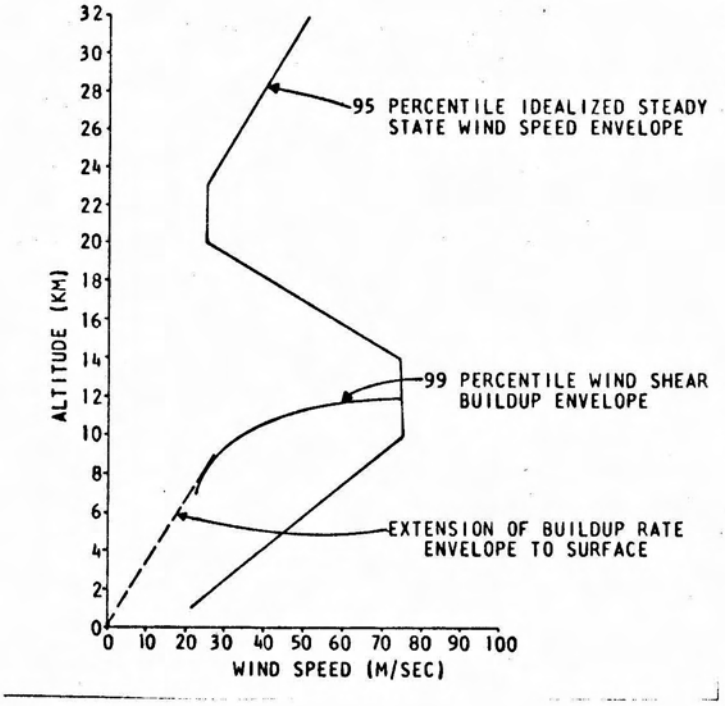

Figure 8. Example of Synthetic Wind Profile Construction

SECTION II. VEHICLE MODEL

The mathematical description of the space vehicle includes a detailed representation of the exciting forces. The exciting forces that make a major contribution to responses are aerodynamics, thrust, and control. Additional requirements for describing the dynamic

characteristics of the vehicle result in equations (Ref. 7) for rigid body motions (translation of center of gravity, y, rotation about center of gravity, φ), and elastic body characteristics (four lateral bending modes, η_μ, six propellant oscillation modes, ξ_s, and engine dynamics, β_E). The control system is represented by the various sensors, shaping networks designed for bending mode stability, and servo-actuator responses. Time variance of vehicle parameters is important. Equations for the vehicle bending moment and unit compression load conclude the model description. A typical Saturn V space vehicle configuration used in the analysis is shown in Figure 9.

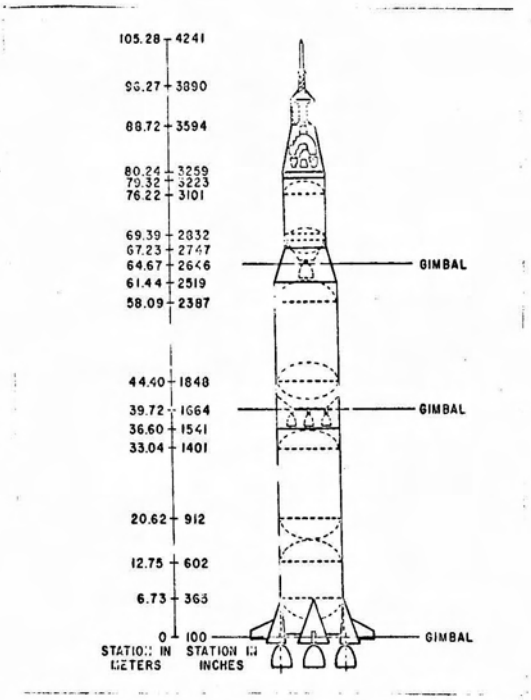

Figure 9. Saturn V Vehicle Configuration

Figure 10 shows the origin of the coordinate system at the undisturbed vehicle center of gravity and its orientation along the tangent to the trajectory pointing in the direction of the nominal thrust vector. The slow rotation of the coordinate system following the trajectory is negligible. Since the vehicle is symmetrical, no cross coupling between pitch and yaw planes is present; hence, a planar analysis is applicable.

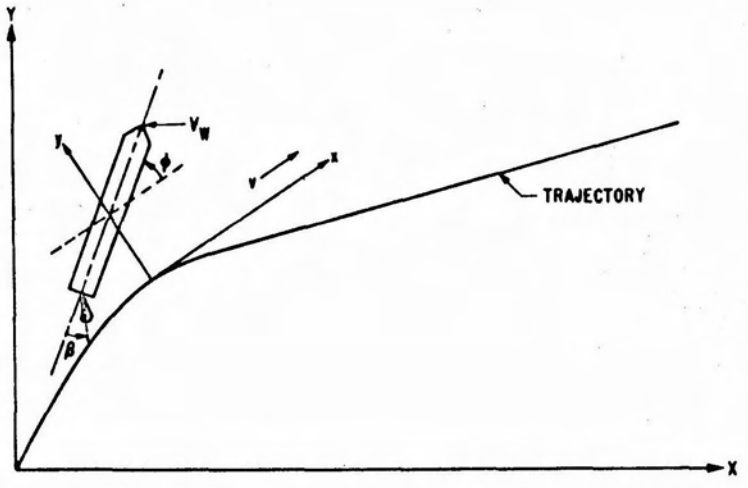

Figure 10. Coordinate System

The aerodynamic forces are quasi-steady, based on normal force distribution, measured or calculated along the longitudinal vehicle axis. This force is considered to vary linearly with the local angle of attack. Because gust penetration and lift growth effects are small for this vehicle configuration, they are neglected.

The bending effects of the launch vehicle structure are approximated by the superposition of several free-free normal mode shapes which define the displacement of the vehicle centerline (Figure 11).

$$y(x,t) = \sum \eta_{\mu}(t)\, y_{\mu}(t) \qquad (1)$$

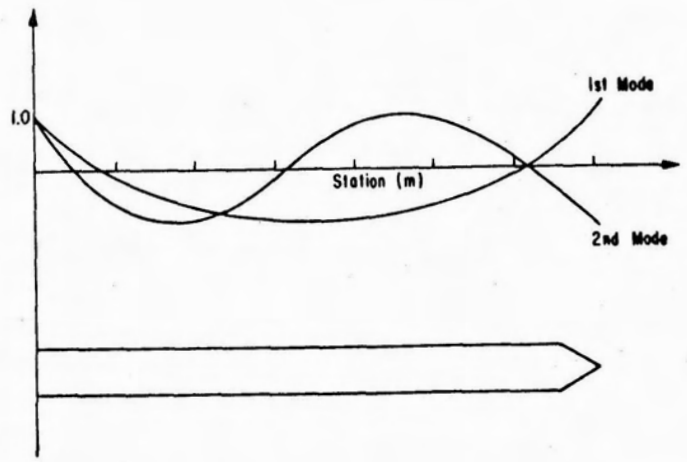

Figure 11. Bending Mode Shapes

Liquid propellant dynamics are represented by a mechanical model for each sloshing mode by springs, dashpots, masses, and inertial discs arranged to produce forces and moments equivalent to original hydrodynamic equations. Only the dynamics of an incompressible, irrotational fluid with small disturbances is included, and only one mode per propellant tank is used.

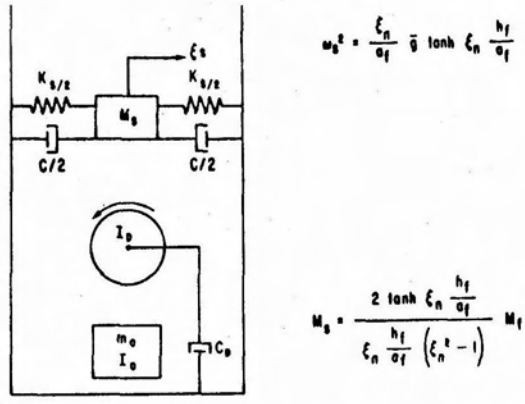

Figure 12. Slosh Model for One Sloshing Mode

Control of the vehicle is maintained by swiveling the engines, using a hydraulic actuator for positioning. The actuator position is determined from a control law formulated to produce desired response and stability characteristics. The control law results from a proper choice of gains attached to the output signal from various control sensors, whose signals are summed and fed directly to the actuators (Figure 13).

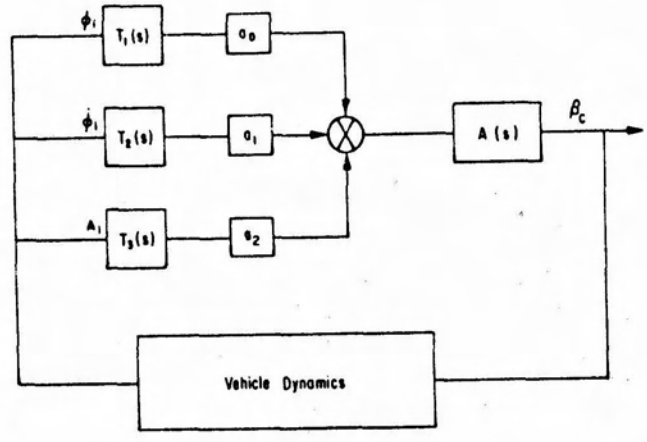

Figure 13. Block Diagram of Control System

The signals from the control sensors are attitude position gyro (φ_i), rate gyro ($\dot{\varphi}_R$), and body-fixed accelerometer (A_i), superimposed with proper gains a_o, a_1, and g_2 according to the control law, β_c.

$$\beta_c = a_o \varphi_i T_1(s) A(s) + a_1 \dot{\varphi}_R T_2(s) A(s) + g_2 A_i T_3(s) A(s). \qquad (2)$$

Sensor dynamics are included in the equations of motion of the total system. Shaping networks are introduced into each channel to stabilize the various vehicle motions. These filters are indicated as $T_i(s)$, and represent the transfer function between input signal and output signal. The transfer function of the actuator is indicated by A(s).

The filters used in this study are as follows:

GYRO	1 IU STA 3235
RATE	$\frac{1}{1 + B_1 S + B_2 S^2}$ STA 2750
ACC	$\frac{1}{1 + 20S}$ IU 3235

Figure 14. Transfer Function of Filters

The system can be reduced to pure gyro control by setting the accelerometer gain g_2 equal to zero. Varying g_2 from zero allows the possibility of load relief and flexibility.

The bending moment or unit compressive load, which results from inertial forces, aerodynamic forces, and engine side forces, can be used as the load indicator. The bending moment equation is

$$M_B(x) = \bar{M}'_\alpha(x)\ \alpha(t) + \bar{M}'_\beta(x)\ \beta(t) + \bar{M}'_{\dot{y}}(x)\ \ddot{y}(t) + \bar{M}'_{\ddot{\varphi}}(x)\ \ddot{\varphi}(t) + \bar{M}'_{\dot{\varphi}}(x)\ \dot{\varphi}(t)$$

$$+ \sum \bar{M}'_{\eta_\mu}(x)\ \eta_\mu(t) + \sum \bar{M}'_{\dot{\eta}_\mu}(x)\ \dot{\eta}_\mu(t) + \sum \bar{M}'_{\ddot{\eta}_\mu}(x)\ \ddot{\eta}_\mu(t)$$

$$+ \sum \bar{M}'_{\ddot{\xi}_s}(x)\ \ddot{\xi}_s(t). \tag{3}$$

Neglecting terms of small magnitude, η_μ, $\dot{\eta}_\mu$, $\dot{\varphi}$, and substituting for the translational and rotational acceleration in terms of their source, allows a simplification of this equation (Ref. 8). The major causes of these accelerations are aerodynamic and control forces. Hence, the transitional acceleration can be expressed as

$$\ddot{y} = \ddot{y}_{aero} + \ddot{y}_{control} = \frac{\partial \ddot{y}}{\partial \alpha}\,\alpha + \frac{\partial \ddot{y}}{\partial \beta}\,\beta. \tag{4}$$

A similar expression for the rotational acceleration is

$$\ddot{\varphi} = \ddot{\varphi}_{aero} + \ddot{\varphi}_{control} = \frac{\partial \ddot{\varphi}}{\partial \alpha}\,\alpha + \frac{\partial \ddot{\varphi}}{\partial \beta}\,\beta. \tag{5}$$

Substituting these expressions (4) and (5) into the bending moment equation (3) results in a simplified expression, which becomes

$$M_B(x) = \overbrace{M'_\alpha(x)\ \alpha(t) + M'_\beta(x)\ \beta(t)}^{\text{Rigid}} + \sum \overbrace{M'_{\ddot{\eta}_\mu}(x)\ \ddot{\eta}_\mu(t)}^{\text{Bending Dynamics}} + \sum \overbrace{M'_{\ddot{\xi}_s}(x)\ \ddot{\xi}_s(t)}^{\text{Sloshing}} . \tag{6}$$

The bending moment equation expressed in this form is superior to the original formulation (3) since various effects, for example, elastic body dynamics, are completely separated. There are additional advantages in satisfying the boundary conditions of zero moment at each end of the vehicle, which are automatically insured by each bending moment partial. This eliminates the differences of large numerical values which are generated simultaneously with the vehicle responses used in equation (3). A typical set of the bending moment coefficients is shown in Figure 15.

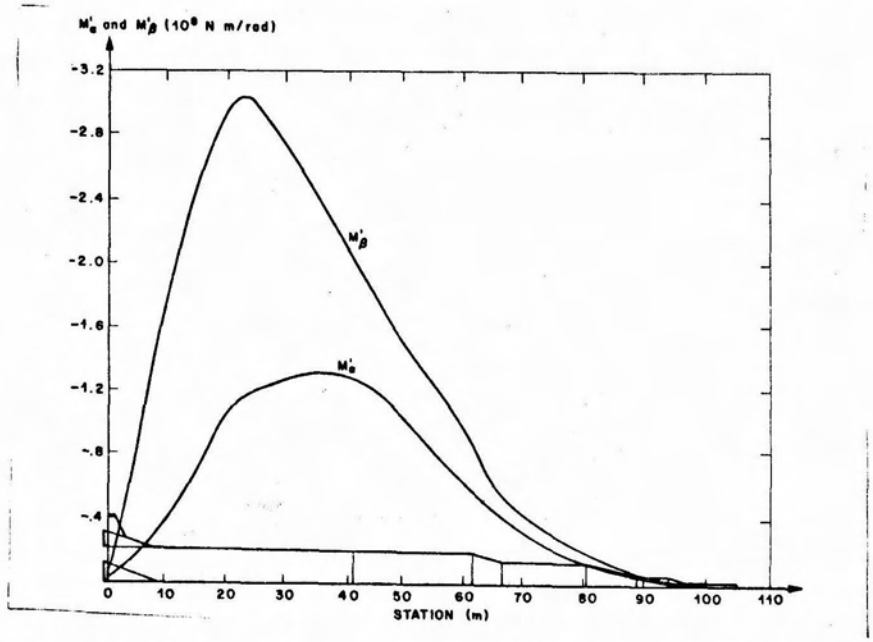

Figure 15. Bending Coefficients for α and β

A more comprehensive load indicator is the total unit compressive load (N_c), which is composed of the longitudinal vehicle acceleration (F/m), the mass ($\bar{m}$) supported above the station of concern, aerodynamic drag (X), and the vehicle bending moment (M_B).

$$N_c(x) = \frac{F(t)\ \bar{m}(x,t)}{m(t)\ \pi D(x)} + \frac{X(x,t)}{\pi D(x)}\left(1 - \frac{\bar{m}(x,t)}{m(t)}\right) + \frac{4M_B(x,t)}{\pi D^2(x)} \quad . \tag{7}$$

D(x) is the local vehicle diameter.

SECTION III. METHODS OF ANALYSIS

Three approaches are used for determining vehicle responses to atmospheric disturbances: (1) numerical integration of equations of motion on a digital computer, (2) integration of equations of motion on an analog computer, and (3) generalized harmonic analysis using spectra of turbulence.

The first method, the digital approach, offers a high degree of accuracy plus sophistication of the vehicle simulation. However, due to the large amount of machine time required for one trajectory simulation (40 minutes of IBM 7094 time), only a few individual wind profiles can economically be studied. These special cases serve as a good cross check on the analog simulation (Ref. 9).

The second method uses a General Purpose high speed analog computer (Ref. 10). Because of the possibility of real time simulation, the analog

is chosen as the basic means of evaluating vehicle responses to many individual detailed wind profiles. Four-hundred trajectory simulations of 2 minutes real-time each can be made in approximately five minutes of computer time. However, computer limitations affect the accuracy and limit the complexity of the analysis, necessitating cross-checks with digital simulation.

Peripheral equipment consists of tape units, noise generators, counters, relays, and oscilloscopes with cameras. The tape units are used for both input and output. The detailed wind profiles, discussed previously, are stored on tape and fed directly into the computer. Output can be stored on an additional tape unit.

Artificial wind turbulence is generated by filtering the output of a white noise generator to satisfy the statistics of the daily variance and turbulence of the wind profiles. The turbulence can be superimposed on a monthly wind mean to obtain an artificial individual wind (Figure 16). While comparable results are obtained by using this

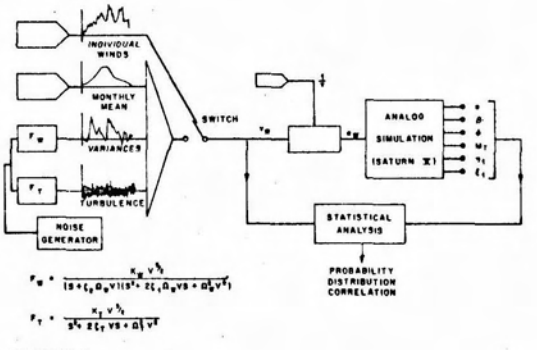

Figure 16. Wind Generation for Analog Computer

generated wind, only the effects of actually measured winds are shown in this analysis.

Statistical probability as a function of magnitude is determined by simulating the flight of the vehicle through all the measured winds and counting the number of profiles in which the response exceeds a preset value. Establishment of the probability levels for any selected response parameter allows a ranking of the severity of the wind profiles. For detailed analysis, particularly interesting wind profiles may be captured on a recorder with closed-loop tape. By placing the computer in a repetitive mode of operation, a given wind profile and its responses can be analyzed in any desired detail.

Generalized harmonic analysis of the vehicle response is the third method used. It allows the statistical qualities of a vehicle response to be computed directly, if certain restrictions are met. The restrictions are linear equations, frozen coefficients over a certain altitude band, and normality of input force. These conditions can be satisfied only for the wind turbulence.

This analysis follows from the stationary random process theory, which states that the mean squared value of a stationary random variable X(t) may be determined very simply if we know the correlation function, $R_x(\tau)$, or the spectral density, $S_x(\omega)$, which corresponds to $R_x(\tau)$. Thus,

$$\bar{X}^2 = R_x(0) = \frac{1}{2\pi} \int_{-\infty}^{\infty} S_x(\omega)\, d\omega. \tag{8}$$

$S_x(\omega)$ (output spectral density) can be shown (Ref. 11) to arise from the relationship between the correlation function of the input and the correlation function of the output as

$$S_x(\omega) = \int_{-\infty}^{\infty} R_x(\tau)\, e^{-i\omega\tau}\, d\tau, \tag{9}$$

where

$$R_x(\tau) = \int_{-\infty}^{\infty} d\rho \int_{-\infty}^{\infty} K(\gamma)\, K(\rho)\, R_m(\tau + \rho - \gamma)\, d\gamma. \tag{10}$$

Therefore, the expression for $S_x(\omega)$ is in the form:

$$S_x(\omega) = |T_x(\omega)|^2 S_{in}\ (\omega). \tag{11}$$

This expression shows that the spectral density, $S_x(\omega)$, of the output of a linear dynamic system is equal to the product of the square of the modulus of its transfer function and the spectral density of the input. Other statistical quantities, exceedances and probability, can be directly calculated from the variance and standard deviation. These statistical values are computed for all vehicle responses for the spectrum of the wind turbulence. The 3σ standard deviation values of the responses were compared with results obtained from the turbulence ensemble.

SECTION IV. PARAMETERS FOR EVALUATION

The assessment of a space vehicle response to atmospheric turbulence cannot be generalized to one vehicle parameter. The optimum design is a compromise between the ability to withstand as large disturbances as possible (particularly wind disturbances), with acceptable control forces and a minimum of structural weight. Depending on the general class of missiles, either the available control forces or the structural loading, or both, will become the critical parameters.

On large liquid-propelled space vehicles like the Saturn V, the weight consideration, which is mainly affected by the structural loading, is usually the most dominant aspect. There is no control problem with this type vehicle since four of the five first-stage engines have control capability. Without this problem, the designer has to deal only with the structural response parameter for optimization of the vehicle. The reduction of structural loads resulting from wind disturbances decreases the vehicle weight and increases payload capability. Operational flexibility is thereby insured because the vehicle can fly more severe trajectories without endangering the mission. For this study, since winds have little effect on longitudinal loads, the bending moment is an adequate load indicator.

SECTION V. FUNDAMENTALS

Two vehicle models are used to illustrate the interaction of exciting force, vehicle dynamics, and control: rigid body response, and total vehicle dynamics. Solutions are obtained for the bending moment using discrete wind inputs.

A. Reaction of a Rigid Vehicle to Atmospheric Loads

As a first step, the problem is restricted to the analysis of a rigid vehicle, and an angle-of-attack feedback is used in the control. The equations for an accelerometer feedback control system can be substituted without difficulty since it is easy to equate accelerometer feedback to angle-of-attack feedback. The equations of motion appear then as

$$\ddot{y} + K_1\varphi + K_2\alpha + K_3\beta = 0 \qquad \text{Translation} \qquad (12a)$$

$$\ddot{\varphi} + c_1\alpha + c_2\beta = 0 \qquad \text{Rotation} \qquad (12b)$$

$$\alpha = \varphi - \frac{\dot{y}}{v} + \alpha_w \qquad \text{Angle of attack} \qquad (12c)$$

$$\beta = a_0\varphi + a_1\dot{\varphi} + b_0\alpha \qquad \text{Control law} \qquad (12d)$$

$$M_B(x) = M'_\alpha(x)\ \alpha(t) + M'_\beta(x)\ \beta(t) \qquad \text{Rigid body bending moment.} \qquad (12e)$$

The solution of these equations giving vehicle responses depends on the solution of the characteristic equation:

$$S\left\{S^3 + S^2\left[a_1c_2 - \frac{b_oK_3}{v} - \frac{K_2}{v}\right] + S\left[c_2(a_o + b_o) + c_1 - \frac{a_1}{v}(c_2K_2 - c_1K_3)\right]\right.$$

$$\left. - \frac{1}{v}\left[-c_1K_1 + a_o(c_2K_2 - c_1K_3) - b_oc_2K_1\right]\right\} = 0. \qquad (13)$$

Assuming that the solution to the above equation has one real root and a pair of complex conjugate roots, i.e.,

$$S_1 = A_1 \qquad (14a)$$

$$S_{2,3} = \sigma \pm i\omega, \qquad (14b)$$

allows the characteristic equation to be written as

$$S\left\{S^3 + S^2(-A_1 - 2\sigma) + S(2A_1\sigma + \sigma^2 + \omega^2) + \left[-A_1(\sigma^2 + \omega^2)\right]\right\} = 0. \qquad (15)$$

The relationship between any of the parameters describing the system can easily be derived using equations (12a) through (15); for example, position gyro gain, rate gyro gain, and drift root can be used as a function of frequency, damping and angle-of-attack meter gain.

This expression for the real root A_1 is

$$A_1 = \frac{\lambda\, c_2B_2 + B_1\lambda^2 + c_2^2\, B_3}{2\lambda\, c_2\, \zeta_c\, \omega_c + \lambda^2 + c_2\, \omega_c^2}\ , \qquad (16)$$

where

$$B_1 = 2\zeta_c \omega_c + \frac{K_2 + b_o K_3}{v} \tag{17a}$$

$$B_2 = -c_1 + \omega_c^2 - c_2 b_o \tag{17b}$$

$$B_3 = -\frac{K_1}{v}(c_1 + b_o c_2) \tag{17c}$$

$$\lambda = \frac{1}{v}(c_2 K_2 - c_1 K_3) \tag{17d}$$

$$\sigma = -\zeta_c \omega_c \tag{17e}$$

$$\omega_c^2 = \sigma^2 + \omega^2. \tag{17f}$$

The dependence of the control frequency, ω_c, on the drift root A_1 and the angle-of-attack gain, b_o, is particularly interesting (Figure 17). It can be seen that A_1 goes positive only as b_o is increased. Control damping has little effect, while increasing control frequency decreases stability of A_1 for small values of ω_c; further increases of ω_c have virtually no effect on A_1. The limiting case of stability occurs when $A_1 = 0$, which is the much published drift minimum condition (Ref. 12), and represents the largest b_o value possible without driving A_1 unstable. To substantially change the real root of the system requires the introduction of angle-of-attack feedback or its equivalent. The changing of this root A_1 has a major influence on vehicle responses, as will be shown in the following results.

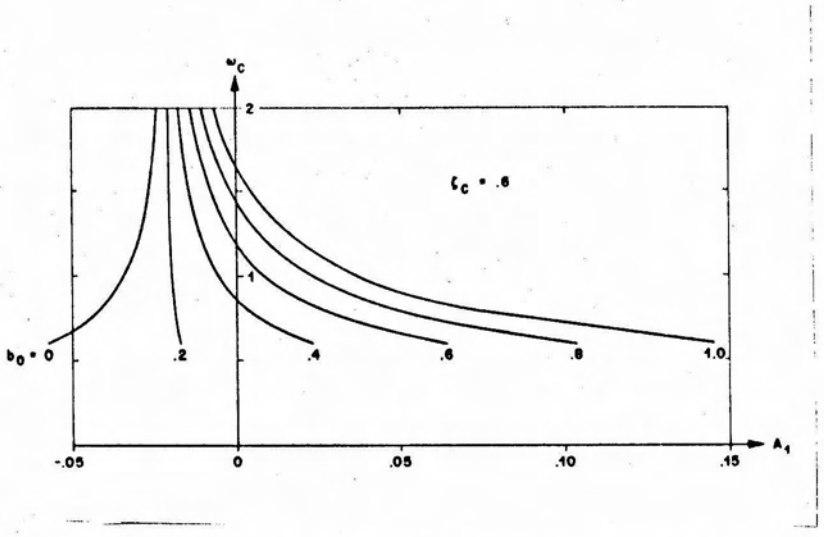

Figure 17. Drift Root vs Control Frequency

Using these roots as parameters, the analytical solutions to the equations were obtained. The solution for a step wind input, $\alpha_w = v_w/v = K$, is given to illustrate certain trends since it very closely approximates the severe gust condition and the gust of the synthetic profile.

$$\alpha(t) = -\frac{K}{\omega}\left[\frac{\left\{c_2a_o + a_1c_2\,\sigma + \sigma^2 - \omega^2\right\}^2 + \omega^2(a_1c_2 + 2\sigma)^2}{A_1^2 - 2\sigma A_1 + \omega^2 + \sigma^2}\right]^{1/2} e^{\sigma t}\sin(\omega t+\varphi_1)$$

$$+\frac{K(A_1^2 + c_2[a_1A_1 + a_o])}{A_1^2 - 2\sigma A_1 + \omega^2 + \sigma^2}\, e^{A_1 t} \qquad (18a)$$

where

$$\psi_1 = \tan^{-1} \frac{(a_1c_2 + 2\sigma)}{c_2(a_o + a_1\sigma + \omega^2 - \sigma^2)} - \tan^{-1}\left(-\frac{\omega}{A_1 - \sigma}\right). \qquad (18b)$$

$$\varphi(t) = \frac{K(c_1 + b_oc_2)}{\omega} \frac{1}{\left[\left(\frac{\omega^2}{\sigma^2 + \omega^2}\right)(A_1^2 - 2\sigma A_1 + \sigma^2 + \omega^2)\right]^{1/2}} e^{\sigma t} \sin(\omega t + \varphi_2)$$

$$- \frac{K(c_1 + b_oc_2)}{A_1^2 - 2\sigma A_1 + \sigma^2 + \omega^2} e^{At} \qquad (19a)$$

where

$$\psi_2 = \tan^{-1}\left(-\frac{\omega}{A_1 - \sigma}\right) - \tan^{-1}\frac{\omega}{\sigma}. \qquad (19b)$$

$$\beta(t) = -\frac{K}{\omega}\left[\frac{\left\{a_oc_1 + a_1c_1\sigma + b_o(\omega^2 - \sigma^2)\right\}^{1/2} + \omega^2(a_1c_1 - 2b_o\sigma)^2}{A_1^2 - 2\sigma A_1 + \omega^2 + \sigma^2}\right]^{1/2} e^{\sigma t}\sin(\omega t + \psi_3)$$

$$+ \frac{K[-A_1^2 b_o + c_1(a_1A_1 + a_o)]}{A_1^2 - 2\sigma A_1 + \omega^2 + \sigma^2} e^{A_1 t} \qquad (20a)$$

where

$$\psi_3 = \tan^{-1} \frac{\omega(a_1c_1 - 2b_o\sigma)}{A_1^2 - 2\sigma A_1 + \omega^2 + \sigma^2} - \tan^{-1} \frac{\omega}{A_1 - \sigma}. \qquad (20b)$$

$$\dot{y}(t) = vK - \frac{Kv\ \omega_c^2\ A_1(-b_y + 1 + A_1)}{A_1^2 - 2\sigma A_1 + \omega^2 + \sigma^2}\ e^{A_1 t}$$

$$- \frac{1}{\omega_c}\left[\frac{\left\{-A_1 + a_y\sigma + 2b_y\sigma^2 - b_y(\omega^2 + \sigma^2)\right\}^2 + \omega^2(-2b_y\sigma - a_y)^2}{\left(\frac{\omega^2}{\sigma^2 + \omega^2}\right)(A_1^2 - 2\sigma A_1 + \omega_c^2)}\right]^{1/2} \tag{21a}$$

$$\cdot\ e^{\sigma t}\ [\sigma \sin(\omega t - \psi) + \omega \cos(\omega t - \psi)]$$

where

$$a_y = \frac{a_1(c_2K_2 - c_1K_3)}{\omega_c^2\ v} \tag{21b}$$

$$b_y = \frac{K_2 - b_oK_3}{\omega_c^2\ v} \tag{21c}$$

$$\psi = \tan^{-1}\left(-\frac{\omega}{A_1 + \sigma}\right) + \tan^{-1}\frac{\omega(-2b_y\sigma - a_y)}{A_1 + a_y\sigma + 2b_y\sigma^2 - b_y(\sigma^2 + \omega^2)} + 2\tan^{-1}\frac{\omega}{\sigma}\ . \tag{21d}$$

The bending moment responses were studied in detail for a typical Saturn V vehicle at a flight time corresponding to the maximum dynamic pressure. Also, control frequency and damping were chosen:

$$\omega_c = 1.2 \text{ rad/sec}$$

$$\zeta_c = 0.6.$$

Defining

$$R(x) = \frac{M'_{\alpha}(x)}{M'_{\beta}(x)}, \tag{22}$$

the bending moment becomes, for gyro control ($A_1 = -0.03$),

$$M_B(x) = -K\, M'_{\beta}(x)\, e^{-0.72t} \left[(0.051R^2(x) + 0.12R(x) + 0.09)^{1/2} \right] \sin(0.882t + \gamma)$$

$$+ K\, M'_{\beta}(x)\, (0.714R(x) + 0.13)\, e^{-0.03t}, \tag{23a}$$

where

$$\gamma = \tan^{-1} \frac{0.22R(x) + 0.3}{0.244R(x) + 0.27}.$$

For the drift minimum case ($A_1 = 0$), the bending moment is

$$M_B(x) = -K\, M'_{\beta}(x)\, e^{-0.72t} \left[(0.174R^2(x) + 0.428R(x) + 0.31)^{1/2} \right] \sin(0.882t + \gamma)$$

$$+ K\, M'_{\beta}(x)\, (0.64R(x) + 0.113), \tag{23b}$$

where

$$\gamma = \tan^{-1} \frac{0.21R(x) + 0.452}{0.359R(x) + 0.332}.$$

Since, for most stations of Saturn V vehicles, $R(x) \leq 0.3$, β contributes the major portion of the transient part of the solution for the bending moment, while angle of attack has more influence on the

quasi-steady-state portion. Changing of the drift root from negative to zero increases the amplitude caused by the transient solution, but decreases the part caused by the drift root. The choice then becomes one of the tradeoff between the transient and steady-state solution. This effect can be related to changing the gains since, by increasing b_o, the drift root becomes more positive; this reduces quasi-steady-state loads but increases transient loads even more. In general, for a rigid vehicle, an overall load reduction is possible by increasing b_o.

B. Elastic Body Reaction to Atmospheric Loads and Control Law

The interplay of total flexible vehicle dynamics with the control law is much more complicated than are the rigid vehicle responses. Transient response becomes more significant for simulations including flexible body dynamics to the extent that load reductions obtained through introduction of alpha control are offset by load increases from flexible body transient loading. To show this effect, the total vehicle dynamics is treated for a synthetic wind profile. The more realistic accelerometer feedback control system is used for this part of the analysis; however, an equivalent with the angle-of-attack control law can easily be established. The effect of bending dynamics on the bending moment is illustrated by splitting the moment into two parts (Ref. 13): that due to rigid body loads,

$$M_{B(\text{rigid})} = M'_{\alpha}(x)\ \alpha(t) + M'_{\beta}(x)\ \beta(t), \tag{24}$$

and that due to elastic body dynamics,

$$M_{B(\text{elastic})} = \sum M'_{\ddot{\eta}_\mu}(x)\,\ddot{\eta}_\mu(t). \tag{25}$$

Figure 18 shows the time response of the rigid body and total (elastic body) bending moment, illustrating the effect of elastic dynamics on the response. The fairly smooth curve represents the contribution from

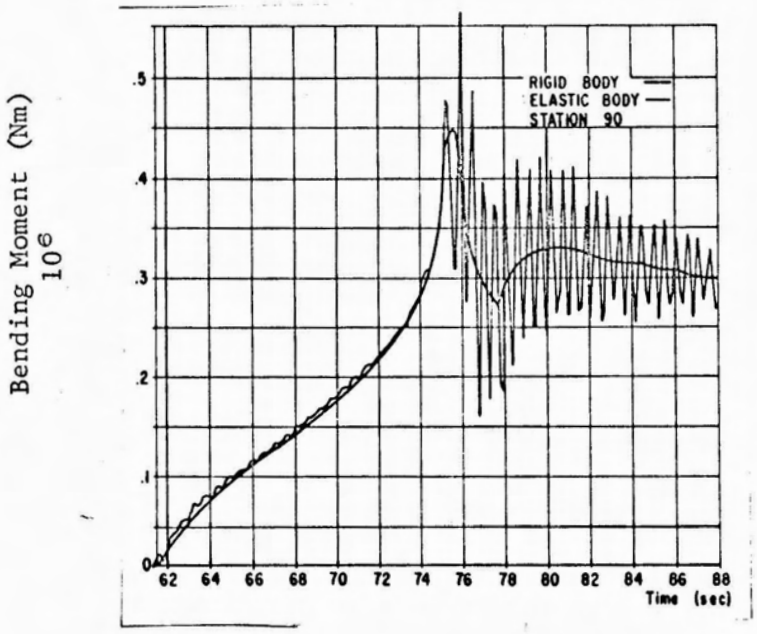

Figure 18. Bending Moment Response (Sta. 90) for Rigid and Elastic Vehicles

rigid body and shows the highly damped transient response resulting from the design profile. The effect of bending dynamics in this region increases the bending moment by 40 percent. This increase can be seen from the total bending moment response that is superimposed over the rigid body bending moment response and is discernible because of the large variance and frequency content.

Because of the small amount of damping present in the vehicle structure, the influence of bending dynamics lasts for a long period of time. This persistence of oscillations can add significantly to the bending moment if cyclic shears are present, particularly if their frequency content occurs near bending mode frequencies.

The ratio of elastic body bending moment to rigid body bending moment was computed by the following:

$$\text{ratio} = \frac{\sum M'_{\ddot{\eta}_\mu}(x)\ \ddot{\eta}_\mu(t)}{M'_\alpha(x)\ \alpha(t) + M'_\beta(x)\ \beta(t)}. \tag{26}$$

The effect is summarized in Figure 19 by plotting the ratio versus vehicle longitudinal stations using accelerometer gain (g_2) as a parameter (Ref. 13).

The bending dynamics effect dominates the load near the upper end of the vehicle, while loads in the first and second stages are dominated by the rigid body . Depending on the vehicle station, the reduction in rigid body loads will be overridden by the increase in

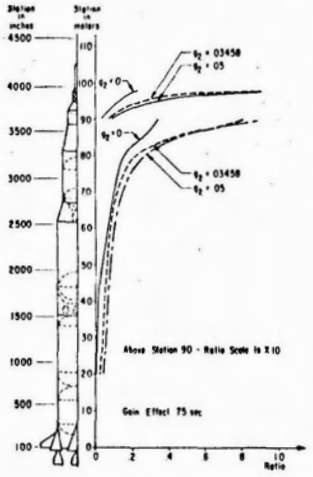

Figure 19. Ratio of Bending Moment Due to Bending Dynamics

the dynamic loading. Increasing the accelerometer gain, g_2, increases the bending dynamic effects while reducing the rigid body effects. This causes a problem in control system optimization. The compromise solution results in a trade-off between the reduction of rigid body loads and increasing elastic loads as g_2 increases.

SECTION VI. RESULTS

A. Individual Profiles

To obtain some insight into the causal relationships between factors contributing to the vehicle loading, the responses of the vehicle to a discrete measured wind profile (Figure 2) were studied first (Ref. 9). Figures 20 and 21 show a direct correlation between effect of the turbulence for specific vehicle stations and the influence of bending dynamics on the bending moments at Station 25.

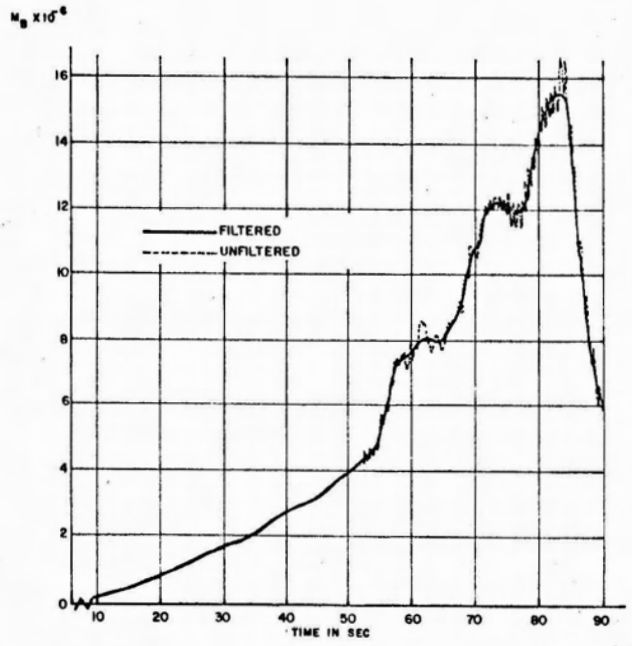

Figure 20. Bending Moment Response (Sta. 25) for Unfiltered and Filtered Wind

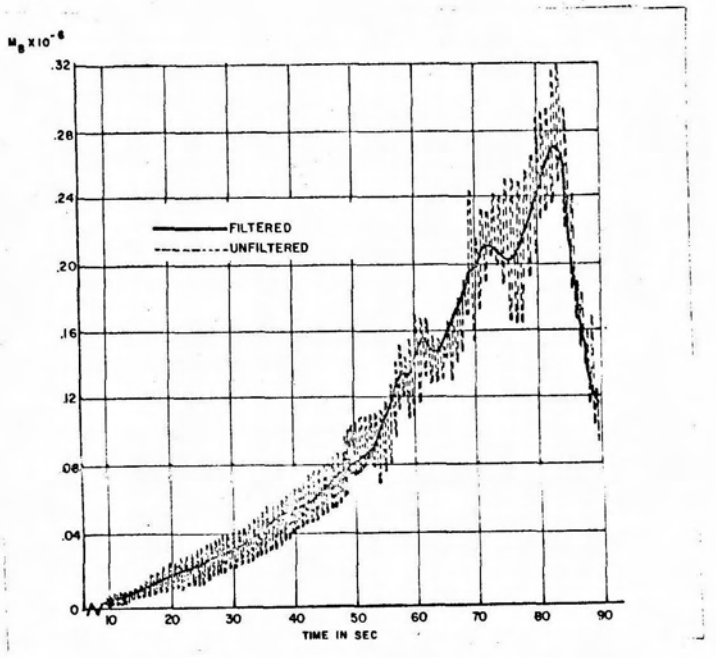

Figure 21. Bending Moment Response (Sta. 90) for Unfiltered and Filtered Winds

Figure 19 shows the bending dynamics contribution to the bending moment to be about 5 percent of the rigid body contribution. As shown in Figure 20, the turbulence increases the bending moment at this station about 7 percent. At station 90, where the bending dynamic effect on the bending moment was about equal to the rigid body effect, turbulence contributed about 20 percent of the total bending moment (Figures 19 and 21).

The influence of short duration wind characteristics is due to two factors: (1) a highly elastic vehicle with low structural damping, and (2) wind disturbances with characteristics that will excite these elastic responses. For the first condition the vehicle elastic

body frequencies are one and two Hz for the first and second bending modes, respectively. The structural damping of these modes is approximately 1/2 percent of critical; however, additional damping (5 percent) is provided by the control system for the first mode. No control damping is introduced in the second mode. The second condition is satisfied in that the wind contains a substantial amount of turbulence at the one to two Hz level (see Figure 4).

The importance of vehicle response to an individual profile cannot be overestimated in application to flight operations procedures, such as prelaunch wind monitoring simulations. However, their application to vehicle design is limited unless a large sample is studied.

B. Ensemble of Wind Profiles

In addition to the single discrete profile case just presented, basic questions arise that the designer must answer. "What is the probability that a vehicle can be launched?" "What are loads for designing the structure that will insure this given launch probability, including the probability of withstanding the environment?" The launch probability can be defined either as an overall probability or the probability of launching during a specific period of the year; for example, the worst wind magnitude month. For this reason, results will be presented for the worst month (March) at Cape Kennedy, Florida and, for the total wind ensembles, unfiltered, filtered and turbulence, being spread over a two-year period. For comparison, additional results are shown on the graphs for the synthetic profile with and without gust.

The probability of a bending moment value not being exceeded in flying through an ensemble of winds is shown on Figure 22 for vehicle station 25 (Ref. 14). The influence of turbulence on this bending moment is small, correlating again the influence of turbulence with the bending dynamics influence on bending moment values. When one probability level of the vehicle response to the turbulence is added to the same probability level of the vehicle response to the filtered ensemble, the resulting value closely approximates the response value obtained for the total ensemble.

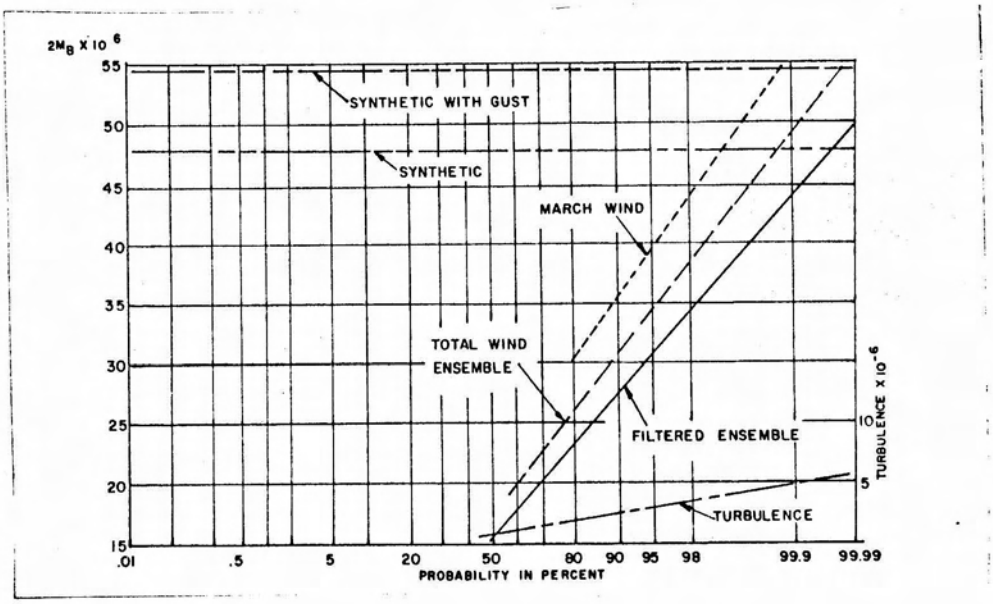

Figure 22. Probability of Bending Moment (Sta. 25) for Wind Ensembles

The synthetic profile with gust produces a response value that has approximately an 0.1 percent probability of being exceeded in terms of the total ensemble, and approximately a 1.0 percent probability in terms of March winds. Similarly, the synthetic profile without gust produces a response value with an 0.1 percent probability of being exceeded in terms of the filtered ensemble.

Results from station 90 (Figure 23) show the same trends. However, the turbulence influence, as was expected, is much higher (30 percent). As has been pointed out, this corresponds to a region with large bending dynamic influence on the bending moment. The spectral density of the turbulence shows a large concentration of energy in the one to two Hz region (Figure 4) indicating the source of bending dynamics excitation.

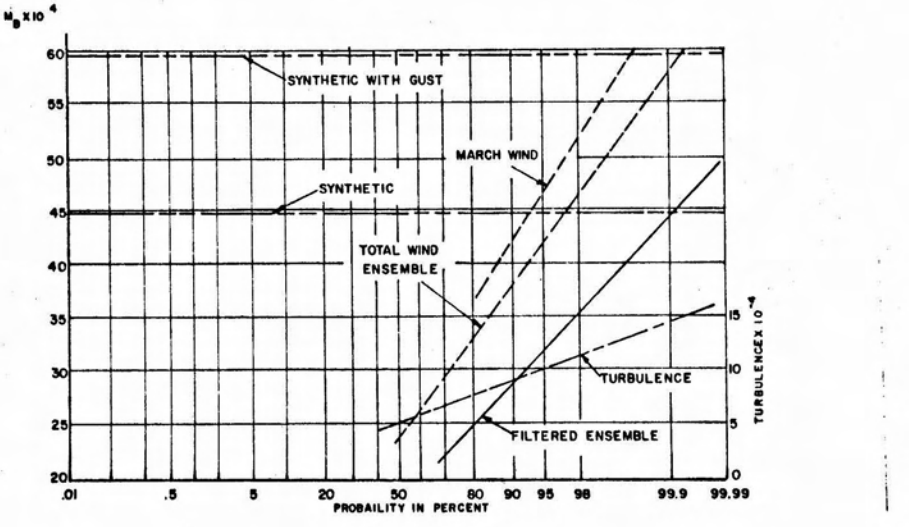

Figure 23. Probability of Bending Moment (Sta. 90) for Wind Ensembles

The total unit compressive load follows the same trend as the bending moment, except that the longitudinal loading dilutes the bending dynamics effect (Figures 24 and 25). At station 25, turbulence contributes only about four percent to the total load. The turbulence contribution to the total load at station 90 is approximately 10 percent.

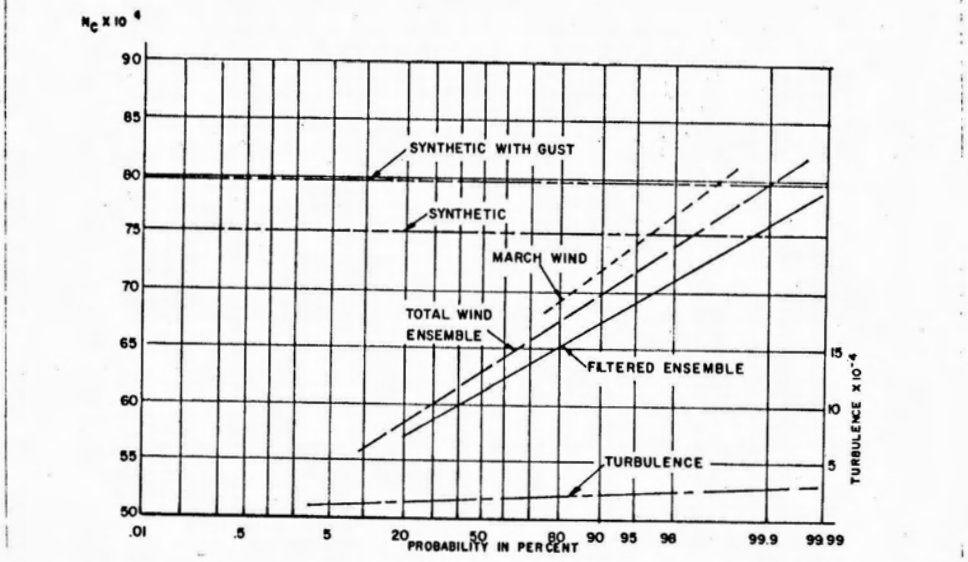

Figure 24. Probability of Total Load (Sta. 25) for Wind Ensembles

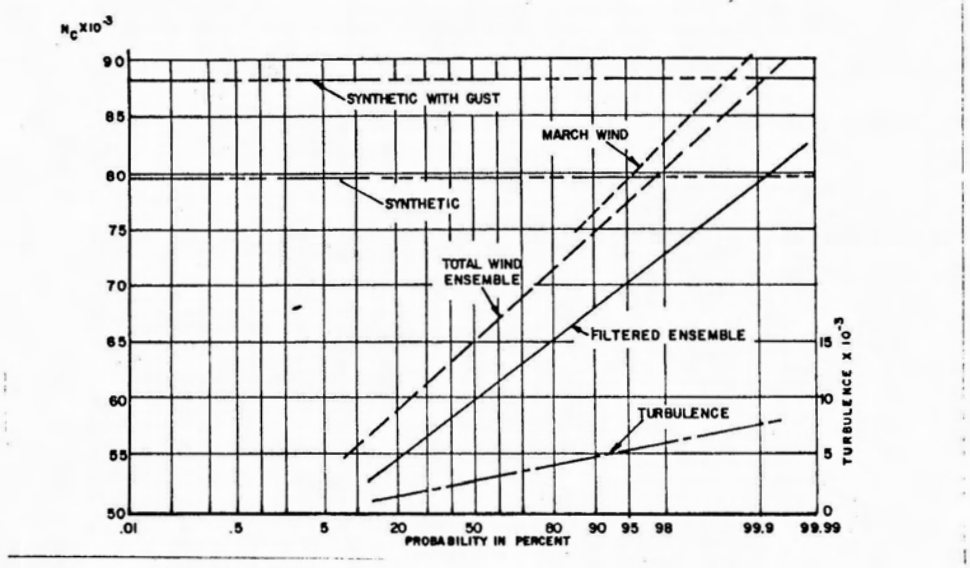

Figure 25. Probability of Total Load (Sta. 90) for Wind Ensembles

A vehicle's bending moment or load can be influenced significantly by wind turbulence (Ref. 15). The amount of influence is determined by the frequency characteristics of the vehicle and of the turbulence. It was shown that, when these frequency conditions were met, the influence of turbulence could be related to the influence of elastic body dynamics on the total bending moment.

C. Severe Profiles

Additional insight into the turbulence effect is gained if profiles causing excessive bending moment values are isolated. Severe profiles were isolated using the bending moment at station 90. Two distinct types of profiles were found: (1) high wind magnitude, moderate wind shears, and (2) moderate wind magnitude, large wind shears. Both types of profiles were severe using the loading at station 90 as an indicator, while only the large wind magnitude profile produced severe loads at station 25.

A typical profile (Figure 26) shows the bending moment at station 25 resulting from the high wind magnitude with only a negligible increase caused by the turbulence (Figure 27). Station 90, for this same wind, shows a higher sensitivity to the turbulence compared to the mean wind magnitude (Figure 28); however, the influence is still moderate, with the large wind speed creating a substantial part of the load.

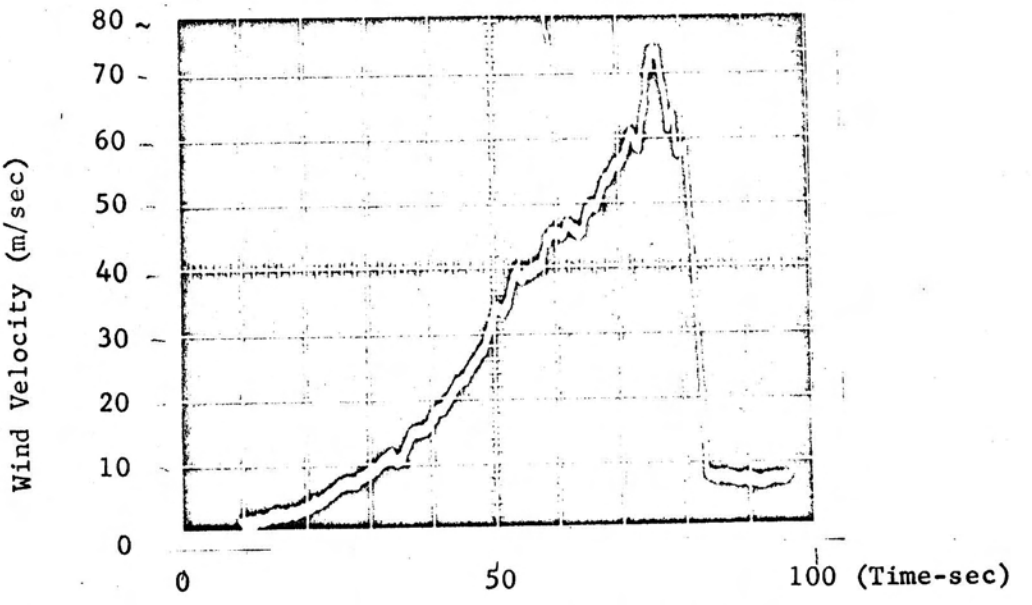

Figure 26. Wind Velocity vs Flight Time

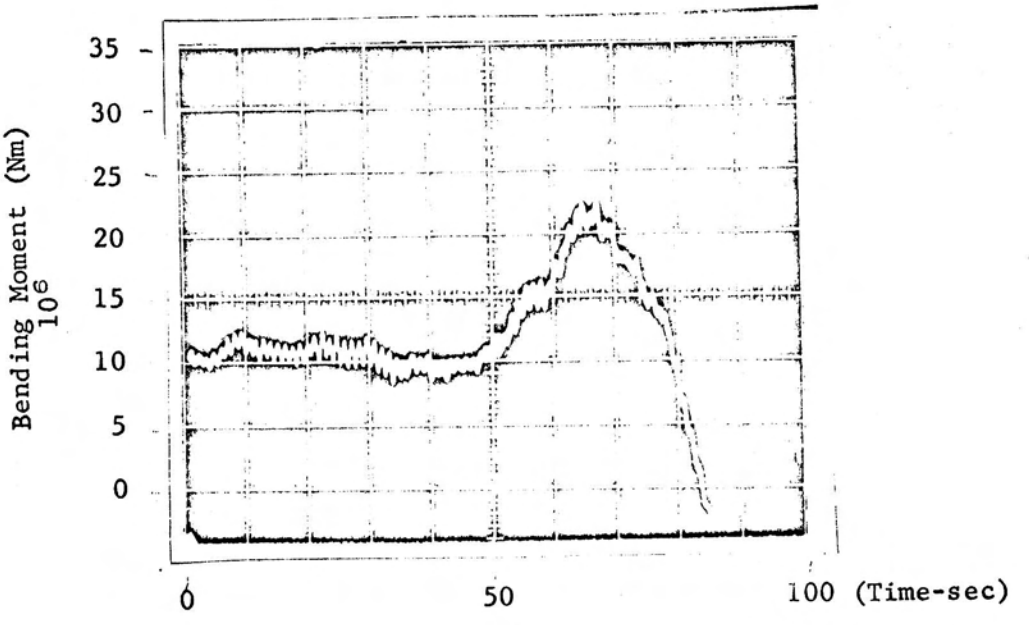

Figure 27. Bending Moment Response (Sta. 25) vs Flight Time

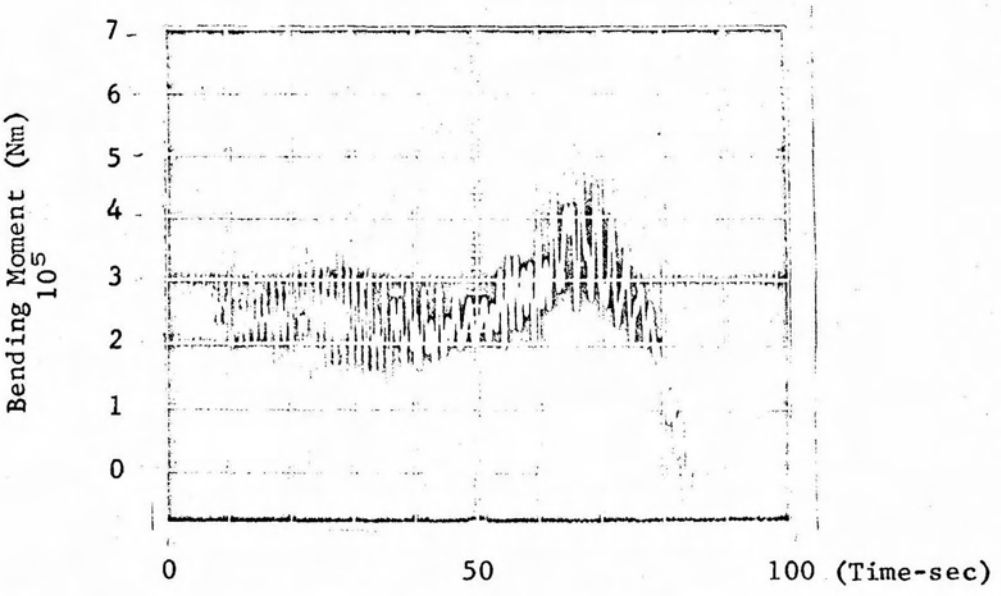

Figure 28. Bending Moment Response (Sta. 90) vs Flight Time

The low wind magnitude, high wind turbulence profile, found to be severe at station 90 (Figures 29, 30 and 31), shows large excitation of the bending dynamics. The small mean wind value of this profile resulted in only a moderate bending moment response at station 25. This particular profile produced the largest bending moment value obtained from the whole ensemble at station 90 (5.2×10^5 Nm). The previous wind (large wind magnitude) produced a bending moment value of 4.8×10^5 Nm at this station. Of the twenty most severe wind profiles for station 90, six were of this low wind speed, large turbulence variety (Figure 29). It is obvious that this type of wind will influence operational procedures. That is, a decision to launch cannot be made on wind measurements alone; it must include prelaunch monitoring. This prelaunch monitoring simulates the vehicle flight through winds

measured during various periods before the predicted launch and determines launch decisions as to structural loads versus structural capability using statistics of wind persistence.

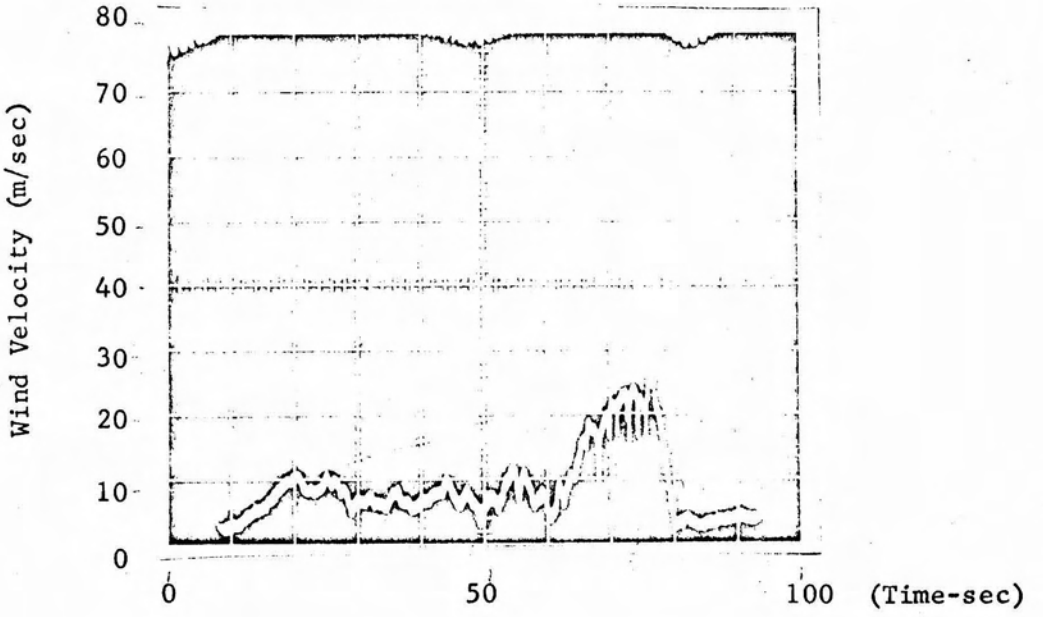

Figure 29. Wind Velocity vs Flight Time

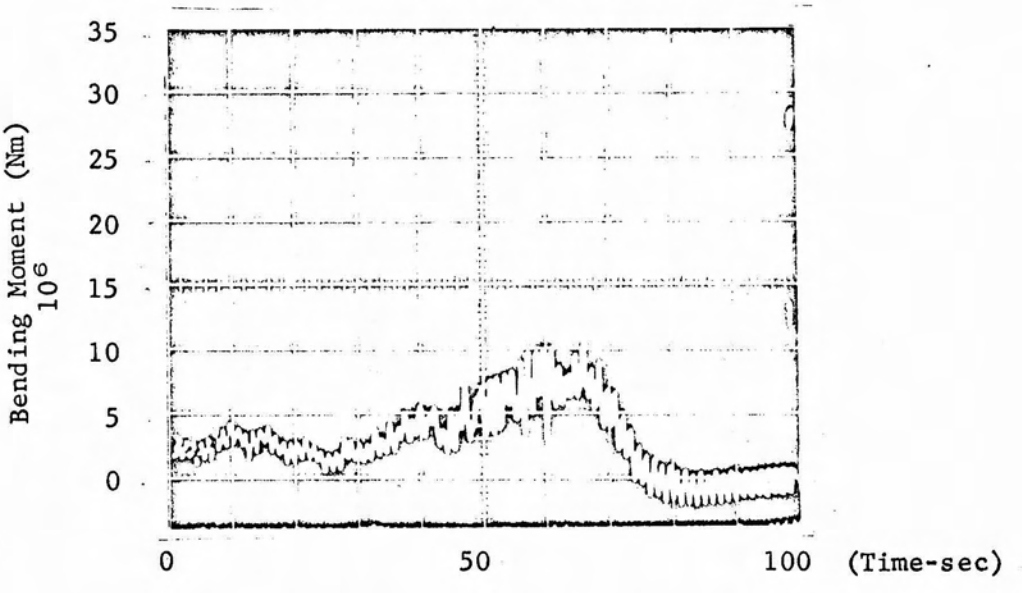

Figure 30. Bending Moment (Sta. 25) vs Flight Time

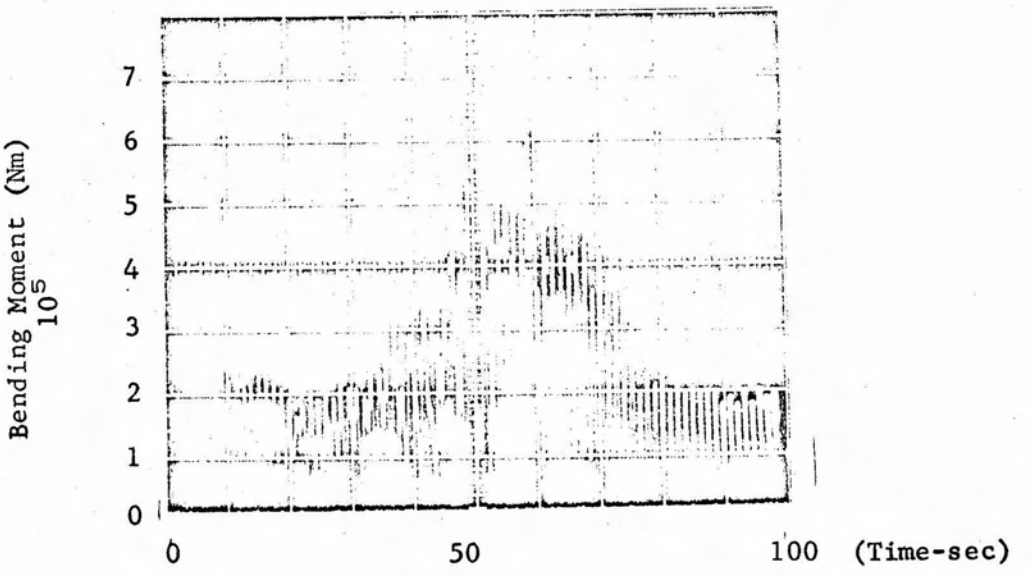

Figure 31. Bending Moment (Sta. 90) vs Flight Time

D. Small Duration Wind Disturbance Effects on Control System Optimization

The influence of wind shears on control system design is more complicated to assess than structural loads. Many factors are important; for example, trade-off of vehicle response versus stability margins. Again, the effect of turbulence on the results corresponds to the region of high bending dynamic influence. Control gains, using an accelerometer optimized for bending moment at station 25, show negligible influence of turbulence, indicating that a reasonable reduction in bending moment can be obtained by increasing the accelerometer gain, g_2. This is illustrated using both the filtered and unfiltered profiles, with both showing approximately the same percentage reduction. The difference in total value is due to the higher peak winds of the unfiltered profiles.

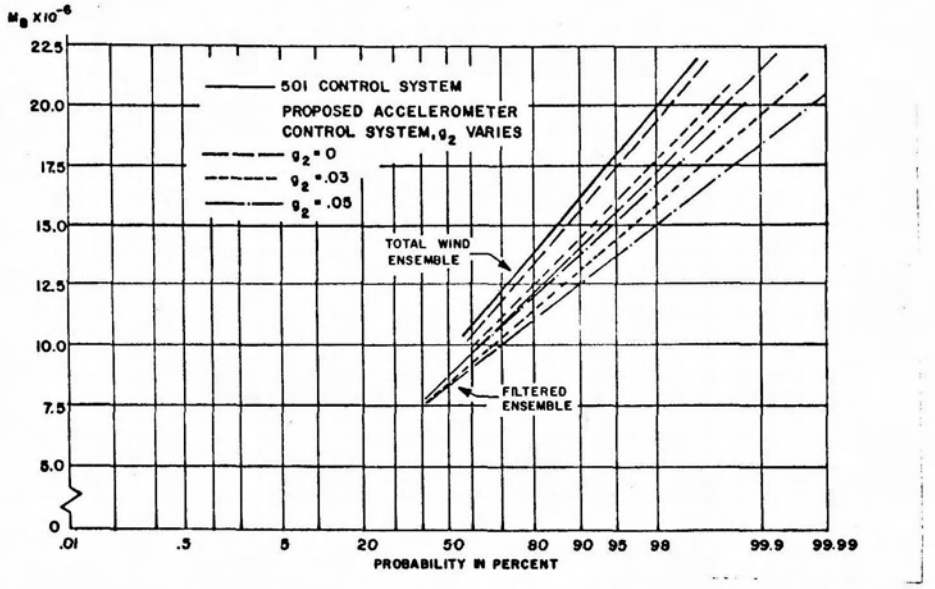

Figure 32. Probability of Bending Moment (Sta. 25) for Wind Ensemble with Accelerometer Gain as Parameter

At station 90, the influence of turbulence is pronounced. Very little reduction in bending moment is possible using the unfiltered profiles; however, the filtered profiles show a good reduction in bending moment as g_2 increases (Figure 33).

The effect is summarized by plotting the 99 percent bending moment value for the three wind ensembles versus the ratio of accelerometer gain to position gyro gain (Figure 34). Also included are the results obtained using the spectrum of the turbulence. This figure shows that increasing the accelerometer gain increases the bending moment for the turbulence profile while decreasing the moment for the unfiltered

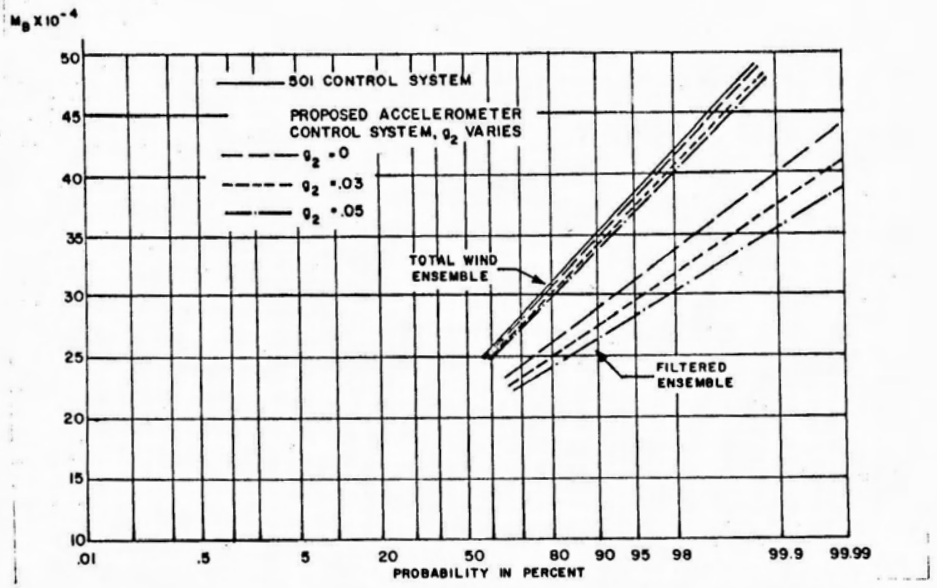

Figure 33. Probability of Bending Moment (Sta. 90) for Wind Ensembles with Accelerometer Gain as Parameter

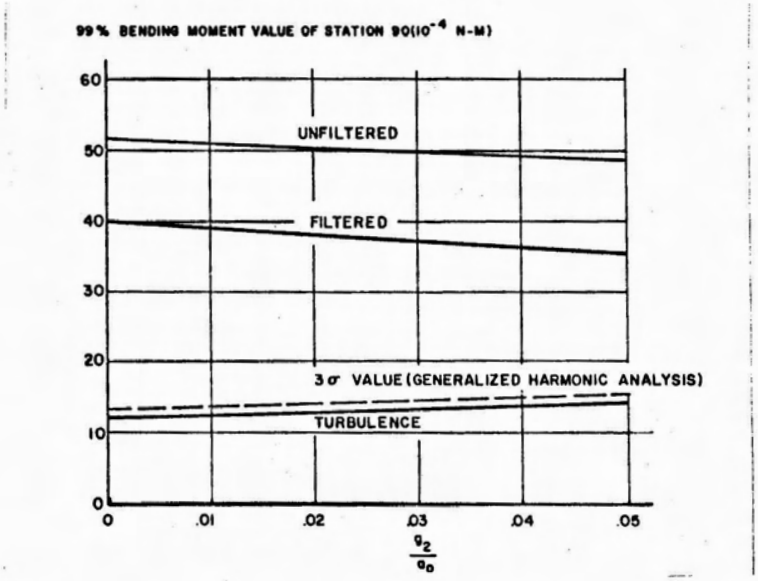

Figure 34. Comparison of Analog Results Using Detailed Wind Profiles with Generalized Harmonic Analysis Using Spectrum for Turbulence

and filtered ensemble, where the reduction is less for the unfiltered ensemble. Turbulence or small shears must be included if control system gains are to be optimized for forward stations. Stations where bending dynamics effects are small show very little change in the optimal gains between the filtered and unfiltered winds. The effect of small scale shears on control system design is therefore dictated by the critical vehicle station for which the gains are to be optimized. In general, this can be determined only after the structure has been designed. At this stage of design, the vehicle response is evaluated and compared to the structural design values indicating weak areas. If the indicated weak areas occur in the forward third of the vehicle, turbulence should be included in final control system optimization.

This approach was used for the Saturn V vehicles, and control system gains optimized for an accelerometer system. Although this system produced some load relief (5 percent), the additional complexity of implementation does not warrant its choice; thus, a gyro system is used.

E. Comparison of Methods

The merits of the different approaches for handling wind inputs have been indicated on previous graphs by showing values obtained from the synthetic profile, with and without gust, unfiltered, filtered and turbulence ensembles, and for generalized harmonic analysis. The following table compares the 99.8 percent values obtained from the ensembles with the synthetic profiles and the spectral analysis for an attitude control system.

Variable	Synthetic w/o Gust	Synthetic w/Gust	Unfiltered	Filtered	Turbulence	Generalized Harmonic Analysis
α	9.8°	11.74°	11.5°	10.3°	0.86°	0.92°
β	1.07°	1.17°	1.05°	1.00°	0.055°	0.035°
$M_B^*(25)$	24	27	25.5	27	2.5	2.8
$M_B^*(90)$	0.45	0.59	0.52	0.4	0.13	0.14

*Bending moment (M_B) given in Nm x 10^6.

The values obtained from generalized harmonic analysis are slightly conservative when compared to the turbulence ensemble with the exception of the engine deflection β. The synthetic profile with gust produced an excessive bending moment at station 90 when compared to the unfiltered ensemble. Otherwise, a good comparison is obtained between the synthetic profile without gust and filtered ensemble, and between synthetic profile with gust and unfiltered ensemble. These results indicate that, for the Saturn V class vehicle, a good structural design could be obtained using almost any combination of approaches which accounted for the gust or turbulence.

The influence of the various methods of handling wind input on optimization of control system is determined by comparing the bending moment at station 90, using various accelerometer gains (g_2).

Acc. Gain g_2	Synthetic w/Gust	Synthetic w/o Gust	Unfiltered	Filtered	Turbulence	Generalized Harmonic Analysis
0	59	44.8	51.5	40	12.5	13.5
0.03	49.5	42	49.5	37.5	13.4	14.4
0.05	46.5	39	48.5	35.5	14.3	15.0

*Bending moment at station 90 given in Nm x 10^4

Comparison of the synthetic profile with the unfiltered wind ensemble at station 25 shows that it is a good representation for gyro control. For drift minimum control ($g_2 = 0.03$), the synthetic profile is a good representation of the bending moment at both stations; however, for gyro control it is too severe at station 90 where there is more sensitivity to turbulence than to wind magnitude. Also, for high load reduction accelerometer gains, the synthetic profile is too optimistic at stations that are sensitive to turbulence. The results indicate that the synthetic profile can be a very useful tool once it has been verified for a particular class of vehicles.

CONCLUSIONS

The results presented in this paper for a Saturn V space vehicle using small scale wind profile effects have indicated several important impacts on space vehicle design.

1. Small scale wind profile effects are important in structural design especially for forward vehicle stations. These are important if the

frequency content of the wind turbulence is near bending mode frequencies or if the shear has the characteristic of a step input.

2. Optimization of control systems should include this small scale wind shear effect in order not to penalize vehicle structural design.

3. Profiles with high wind speeds and moderate wind shears create high structural loads at all stations; however, a profile with low wind speeds but high wind shears can create large loads when the influence of bending dynamics is high.

REFERENCES

1. Dvoskin, Norman and Norman Sissenwine, "Evaluation of AN/GMS-2 Wind Shear Data for Development of Missile Design Criteria," Air Force Surveys in Geophysics, No. 99, 1958.

2. Eckstrom, Clinton V., "Theoretical Study and Engineering Development of Jimsphere Wind Sensor," Final Report, NASA Contract NAS8-11158, G. T. Schjeldahl Company, Northfield, Minnesota, July 1965.

3. Rogers, R. R. and H. G. Camitz, "Project Baldy, An Investigation of Aerodynamically-Induced Balloon Motions," Final Report, NASA Contract NAS8-11140, Cornell Aeronautical Laboratory, Inc., Buffalo, New York, April 1965.

4. Scoggins, James R. and Michael Susko, "FPS-16 Radar/Jimsphere Wind Data Measured at the Eastern Test Range," NASA TM X-53290, MSFC, 1965.

5. Scoggins, James R., "Spherical Balloon Wind Sensor Behavior," J. Appl. Meteor., 4, 1965.

6. Daniels, Glenn E., et al., "Terrestrial Environment (Climatic) Criteria Guidelines for Use in Space Vehicle Development, 1966 Revision," NASA TM X-53328, MSFC, 1966.

7. Rheinfurth, Mario H., "Control-Feedback Stability Analysis," DA-TR-2-60, 11 January 1960.

8. Townsend, Don, "A Method for the Determination of Control Law Effect on Vehicle Bending Moment," NASA TM X-53077, July 2, 1964.

9. Townsend, Don, "Saturn V Wind Response Studies," NASA MTP-AERO-63-63, MSFC, Sept. 10, 1963.

10. Ryan, Robert S. and Dieter Teuber, "A Practical Approach to the Optimization of the Saturn V Space Vehicle Control System Under Aerodynamic Loads," NASA TM X-53298, MSFC, July 21, 1965.

11. Bendat, Julius S., Principles and Applications of Random Noise Theory, John Wiley and Sons, Inc., New York, 1958.

12. Geissler, Ernst D., "Problems in Attitude Stabilization of Large Guided Missiles," DA-TR-21-60, 13 June 1960.

REFERENCES (Continued)

13. King, Alberta C., "The Effect of Bending Dynamics and Control Gain on the Bending Moment," NASA TM X-53387, MSFC, February 7, 1966.

14. Ryan, Robert S. and Harry Harcrow, "A Technique for Analyzing Control Gains Using Frequency Response Methods," AIAA Paper No. 66-484, presented at the 4th Aerospace Science Meeting, Los Angeles, California, June 27-29, 1966.

15. Bieber, R. E., "Relative Influence of Atmospheric Properties on Space Vehicle Design," AMS-AIAA Conference on Aerospace Meteorology, Los Angeles, California, March 28-31, 1966.